TECHNICAL REVIEW

Dyn-X Technology
Order Tracking
Comparison of **IBEM**
PNAH and **LDV** Methods

No.1 2006

Brüel & Kjær

Previously issued numbers of Brüel & Kjær Technical Review

1 – 2005 Acoustical Solutions in the Design of a Measurement Microphone for Surface Mounting
Combined NAH and Beamforming Using the Same Array
Patch Near-field Acoustical Holography Using a New Statistically Optimal Method
1 – 2004 Beamforming
1 – 2002 A New Design Principle for Triaxial Piezoelectric Accelerometers
Use of FE Models in the Optimisation of Accelerometer Designs
System for Measurement of Microphone Distortion and Linearity from Medium to Very High Levels
1 – 2001 The Influence of Environmental Conditions on the Pressure Sensitivity of Measurement Microphones
Reduction of Heat Conduction Error in Microphone Pressure Reciprocity Calibration
Frequency Response for Measurement Microphones – a Question of Confidence
Measurement of Microphone Random-incidence and Pressure-field Responses and Determination of their Uncertainties
1 – 2000 Non-stationary STSF
1 – 1999 Characteristics of the vold-Kalman Order Tracking Filter
1 – 1998 Danish Primary Laboratory of Acoustics (DPLA) as Part of the National Metrology Organisation
Pressure Reciprocity Calibration – Instrumentation, Results and Uncertainty
MP.EXE, a Calculation Program for Pressure Reciprocity Calibration of Microphones
1 – 1997 A New Design Principle for Triaxial Piezoelectric Accelerometers
A Simple QC Test for Knock Sensors
Torsional Operational Deflection Shapes (TODS) Measurements
2 – 1996 Non-stationary Signal Analysis using Wavelet Transform, Short-time Fourier Transform and Wigner-Ville Distribution
1 – 1996 Calibration Uncertainties & Distortion of Microphones.
Wide Band Intensity Probe. Accelerometer Mounted Resonance Test
2 – 1995 Order Tracking Analysis
1 – 1995 Use of Spatial Transformation of Sound Fields (STSF) Techniques in the Automative Industry
2 – 1994 The use of Impulse Response Function for Modal Parameter Estimation
Complex Modulus and Damping Measurements using Resonant and Non-resonant Methods (Damping Part II)
1 – 1994 Digital Filter Techniques vs. FFT Techniques for Damping Measurements (Damping Part I)
2 – 1990 Optical Filters and their Use with the Type 1302 & Type 1306 Photoacoustic Gas Monitors

(Continued on cover page 3)

Technical Review

No. 1 – 2006

Contents

TRADEMARKS

ICP is a registered trademark of PCB Group
DeltaTron is a registered trademark and PULSE is a trademark of Brüel & Kjær Sound & Vibration Measurement A/S

Editor: Harry K. Zaveri

Dyn-X Technology: 160 dB in One Input Range

Niels-Jørgen Jacobsen, Ole Thorhauge Andersen

Abstract

The dynamic range of high-quality measurement accelerometers and microphones has for many years been significantly better than that of the analog signal conditioning electronics and analog-to-digital converters (ADCs) of the data acquisition systems. This is despite the fact that data acquisition systems today are typically based on 24-bit ADCs, and theoretically able to handle signal dynamics of up to 144 dB. In practice, however, most of these ADCs do not have a useful dynamic range higher than 100 – 110 dB. Consequently, great care must be exercised in optimising the analysis chain dynamics to the output of the transducer, in order to avoid overload and under-range situations. This article describes some of the analysis chain imperfections that are present in data acquisition systems and how a high dynamic operating range can be achieved, in a single input range, using state-of-the-art designs.

Résumé

Les microphones et les accéléromètres de mesure haut de gamme connectés aux systèmes d'acquisition de données ont depuis de nombreuses années une dynamique supérieure à celle des conditionneurs analogiques et des convertisseurs A-N. Et ce, en dépit du fait que les systèmes d'acquisition actuels intègrent des convertisseurs 24 bits dont la dynamique peut, en théorie, atteindre 144 dB. Or, dans la pratique, il s'avère que la gamme de mesure utile de ces convertisseurs ne dépasse pas 100 – 110 dB. Pour éviter les situations de surcharge et de valeurs sous-gamme, il faut donc préalablement minutieusement faire correspondre la dynamique de la chaîne de mesure au signal de sortie du capteur. Cet article traite de certaines des imperfections de la chaîne d'analyse inhérentes aux systèmes d'acquisition de données et des moyens qui permettent d'obtenir une dynamique de mesure élevée pour une gamme d'entrée spécifique.

Zusammenfassung

Der Dynamikbereich hochwertiger Beschleunigungsaufnehmer und Messmikrofone ist viele Jahre lang wesentlich besser gewesen als der Dynamikbereich der Elektronik für die analoge Signalkonditionierung und der A/D-Wandler der Messwerterfassungssysteme. Dies gilt ungeachtet der Tatsache, dass Messwerterfassungssysteme heute in der Regel 24-Bit A/D-Wandler verwenden und theoretisch eine Signaldynamik bis 144 dB bewältigen. In der Praxis besitzen die meisten dieser A/D-Wandler jedoch einen nutzbaren Dynamikbereich, der 100 – 110 dB nicht überschreitet. Aus diesem Grund muss die Dynamik der Analysekette sehr sorgfältig auf das Ausgangssignal des Sensors abgestimmt werden, um Übersteuerungen und Bereichsunterschreitungen zu vermeiden. Dieser Artikel beschreibt Unzulänglichkeiten der Analysekette, die in Messwerterfassungssystemen auftreten, und wie sich mit Hilfe einer innovativen Bauart ein hoher Dynamikbereich mit einem einzigen Messbereich erreichen lässt.

Introduction

The system performance that can be expected of present and future analysis systems is described in this article.

First, a definition of dynamic operating range and dynamic range is given, followed by some practical considerations regarding the potential dynamic range of high-quality transducers and a brief overview of the factors that reduce the system performance to less than the theoretical limit.

Then, a few theoretical considerations regarding the potential dynamic range of a digital system, and the potential improvements when using narrowband analysis, are provided.

Finally, a new technology optimising the dynamic operating range of the system is introduced and illustrated with measurements showing system performance of 160 dB or more when using narrowband analysis.

Dynamic Operating Range, Dynamic Range and Frequency Bandwidth

The ratio between the highest and lowest signal a system can measure overall is defined as the dynamic operating range of the system. The ratio between the highest signal a system can measure in a given input range and the system base noise for the same input range is defined as the dynamic range of the system for the given

input range. If the dynamic range is too low, then high signals will be clipped and distorted while low signals will be buried in system noise. In technical terms, the dynamic range (*DR*) is the ratio between the RMS value of a full-scale sine wave V_{FS} and the RMS value of the system base noise V_N. It is typically given in dB:

$$DR = 20 \times \log \frac{V_{FS}}{V_N} \tag{1}$$

When discussing dynamic range, the frequency bandwidth of the measurement must be taken into consideration. In a well-designed system the inherent system noise can be characterised as white noise. Consequently, if all elements of the measurement chain are linear in nature, the dynamic range of the measurement can be improved by reducing the measurement frequency bandwidth. This is actually one of the advantages of the commonly used FFT analysis. For the above statement to be valid, it is essential that no artifacts are introduced in either the time domain or the frequency domain, when performing narrowband analysis.

Dynamic Range of Transducers

For the last 30 to 40 years, sound and vibration transducers have outperformed the subsequent analysis systems as regards linearity and dynamic performance. A high-quality transducer, including preamplifier, can deliver a practically noise-, spurious- and distortion-free signal over a dynamic range of 120 to 130 dB using broadband, and 160 dB using narrowband, analysis. In a well-designed transducer, the limiting factors for achieving a high dynamic range are mainly the noise floor and the clipping level of the pre-amplifier's electronics. The transducer element itself does not limit the performance.

The noise floor V_N of a high-quality preamplifier has for the last 30 to 40 years been in the region of 3 μV to 15 μV in the audible frequency range and the maximum linear output V_{FS} of a DeltaTron®/ICP® transducer is 5 V_{RMS} (7.071 V_{peak}). Table 1 provides examples of dynamic ranges that can be expected for a high-quality transducer.

Throughout this article a bandwidth of 25.6 kHz is used for broadband comparisons. For narrowband comparisons 24 Hz, 6 Hz and 1 Hz are used, where, for example, 6 Hz corresponds to the effective noise bandwidth of a 25.6 kHz FFT analysis with 6400 lines using Hanning weighting [1]. So, a high-quality transducer can be used for narrowband measurements over a dynamic range of 160 dB (effective noise bandwidth 6 Hz) given that no other factors affect the measurement chain.

Table 1. Dynamic ranges for a high-quality DeltaTron/ICP transducer

Bandwidth (Hz)	25 600	1 024	24	6	1
V_{FS} (V_{RMS})	5				
V_N (V_{RMS})	3 μ	600 n	92 n	46 n	19 n
DR (dB)	124	138	155	161	169

Analysis Chain Imperfections

The clipping level and the noise floor are not the only factors limiting the useful dynamic range of the analysis system. The list below includes some other factors that limit the analysis system performance.

Harmonic Distortion: Signals caused by non-linearities in the analog signal conditioning. Typically characterised as a family of harmonic components, where the levels are determined relative to the measurement signal.

Cross-talk: Signals caused by inter-channel coupling, where the levels are determined relative to the signal level of the originating channel.

Spurious: Signals caused by various phenomena such as power supply imperfections, clock circuits, bus communication and EMC coupling between circuits.

ADC Resolution: The ADC resolution is given by the number of bits N as 2^N.

ADC Non-linearity: Digital distortion components caused by uneven quantisation step sizes in the ADC.

Aliasing: Signal artifacts originating from signal components of frequencies higher than the Nyquist frequency, where the levels are determined relative to the measurement signal.

DSP Imperfections: Modern analysis systems perform filtering, decimation and the actual analysis in the digital domain. Throughout the whole digital analysis chain a high dynamic range requires high-speed calculations of high accuracy. High-speed DSPs are both expensive and have high power consumption.

System Considerations

No system is better than the weakest link in it's chain. The analysis chain consists of coupled elements each with a limited dynamic range as illustrated in Fig. 1.

Fig. 1. Example of dynamic ranges of an analysis chain

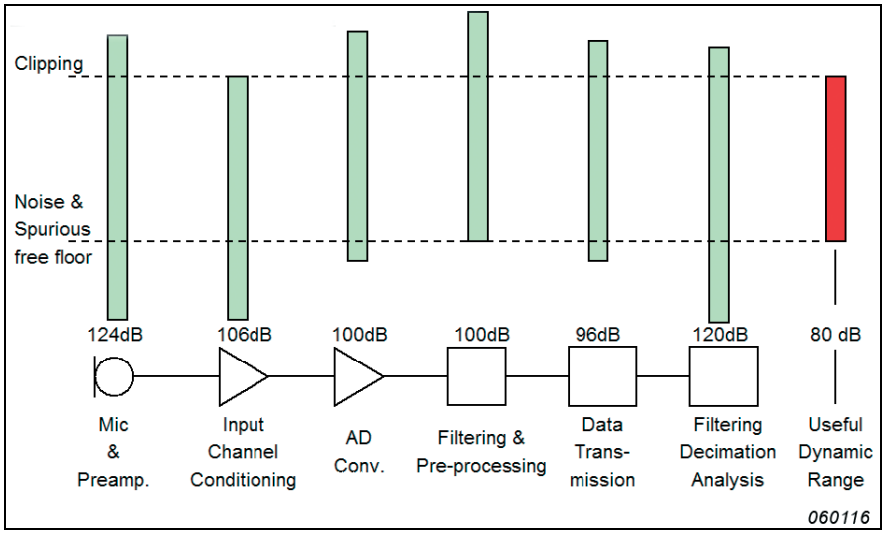

The ADC has been the weakest link in the analysis chain ever since the invention of digital signal processing. New ADC designs have, however, improved performance dramatically. Table 2 gives a rough overview of the historical evolution in ADC specifications for sound and vibration analysis. Traditional ADC designs still lack performance when compared to the transducer (Table 1).

Table 2. A historic overview of specifications of ADCs. F_s: Sampling frequency

Year	ADC Resolution (bits)	Dynamic Range (DC – F_s/2) [dB]
1970	10 – 12	60 dB
1980	14 – 16	70 dB
1990	16	80 dB
2000	24	100 dB
2005	24	110 dB

Overcoming the Analysis Chain Imperfections

The fact that the transducer has historically always outperformed the subsequent elements of the analysis chain with respect to dynamic range, has been compensated for by the inclusion of an input attenuator in the analysis chain. This has, in practice, compensated for the limited dynamic range of the ADC and also the limitations in the following DSP chain by increasing the dynamic operating range. The drawback is, however, quite a high risk of bad measurements as overload and under-range situations can occur (Fig. 2).

Fig. 2. Illustration showing the effect of using an input attenuator for sound measurements

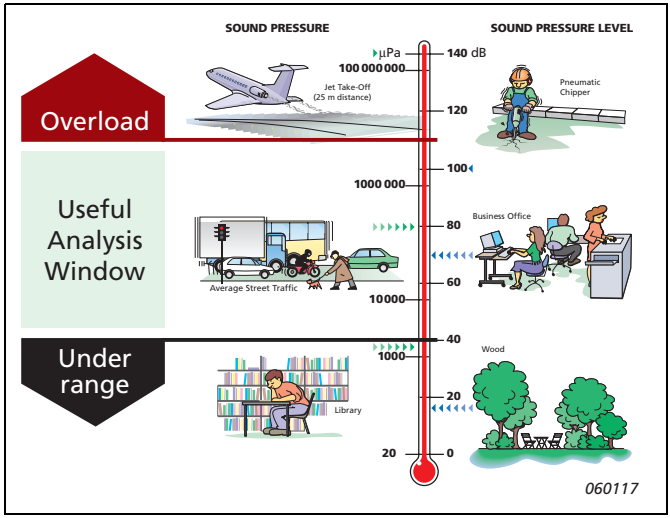

An overloaded measurement is erroneous and has to be re-measured. There is no way of estimating the correct result. Overloads are probably the greatest cause of bad measurement results. This issue is even more critical in multi-channel and/or multi-analysis measurements, as it is more difficult to get an overview of the whole measurement scenario and avoid erroneous measurements.

Theoretical Dynamic Range of a 24-bit System

An approach similar to the one applied to the transducer can be applied to the system with respect to broadband and narrowband analysis. The theoretical dynamic range in dB, can be calculated as [2]:

$$DR = 20 \times \log\left(2^N \times \sqrt{\frac{F_s}{2 \times F_{NBW}}}\right) \quad (2)$$

where N is the system quantisation in bits, F_S is the sampling frequency and F_{NBW} the effective narrowband analysis bandwidth in Hz.

Careful system design can ensure that the quantisation noise is, theoretically, random and thus with a uniform spectral density (white). Under this assumption, the theoretical dynamic range in dB, can be calculated as [2]:

$$DR = 20 \times \log\left(2^N \times \sqrt{\frac{F_s}{2 \times F_{NBW}}} \times \sqrt{1.5}\right) \quad (3)$$

giving an increased dynamic range of approximately 1.8 dB compared to equation (2).

Using equation (2) table 3 shows the dynamic range in different bandwidths as a function of system quantisation.

Table 3. Theoretical dynamic ranges for different system quantisation and bandwidth using equation (2). F_s = 65 536 Hz

N (bits)	Resolution	Dynamic Range				
		F_{NBW} (Hz)				
		32 768	1 024	24	6	1
16	65 536	96	111	128	134	141
20	1 048 576	120	135	152	158	166
24	16 777 216	144	160	176	182	190

Using equation (2) or equation (3), the theoretical increase in dynamic range ΔDR can be expressed as a ratio between the sampling frequency F_s and the width of the narrowband analysis F_{NBW} [2]:

$$\Delta DR = 20 \times \log \sqrt{\frac{F_s}{2 \times F_{NBW}}} \quad (4)$$

Table 4. Theoretical increase in dynamic range, ΔDR. F_s = 65 536 Hz

F_{NBW} (Hz)	1 024	24	6	1
DR (dB)	15	31	37	45

Narrowband analysis can improve the dynamic range quite dramatically and an ideal 24-bit system can fully match the performance of modern transducers.

Introduction of New Technology

The above discussion shows that if the ADC performance can be significantly improved in combination with a careful design of the whole analysis chain, then the problematic input ranging can be eliminated. Brüel & Kjær have researched this over the years and have recently introduced a new technology designed to increase the dynamic performance of the whole analysis chain sufficiently to eliminate the use of input attenuators.

Dyn-X Technology

This new technology is called Dyn-X. In brief, the technology utilises a specialised analog input design to provide a very high dynamic range of the analog circuit, pre-conditioning the transducer signal before feeding it to the ADC. The Dyn-X input channels have no input attenuators, but a single input range from 0 to 10 V_{peak}. The digitising is performed synchronously in two specially selected, high-quality, 24-bit delta-sigma ADCs, and both data streams are fed to the DSP environment where dedicated algorithms in real-time merge the signals while obtaining an extremely high-accuracy match in gain, offset and phase. An important requirement of the design process was that no technical drawbacks must be introduced in either the time or the frequency domain with respect to distortion and other artifacts, when compared to existing designs (Fig. 3).

Fig. 3. A simplified block diagram of the Dyn-X technology

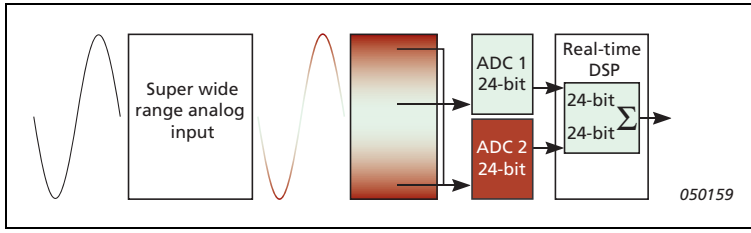

Fig. 4. Comparison of dynamic performance for standard 24-bit input channel (Std.), the Dyn-X input channel (Dyn-X) and a high-quality transducer. Analysis bandwidth: 25.6 kHz

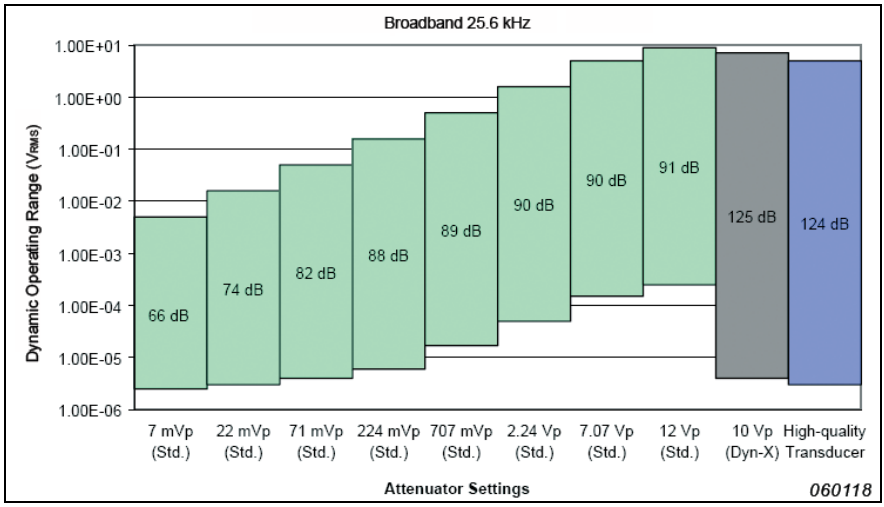

Fig. 5. Comparison of dynamic performance for standard 24-bit input channel (Std.), the Dyn-X input channel (Dyn-X) and a high-quality transducer. Analysis bandwidth: 6 Hz

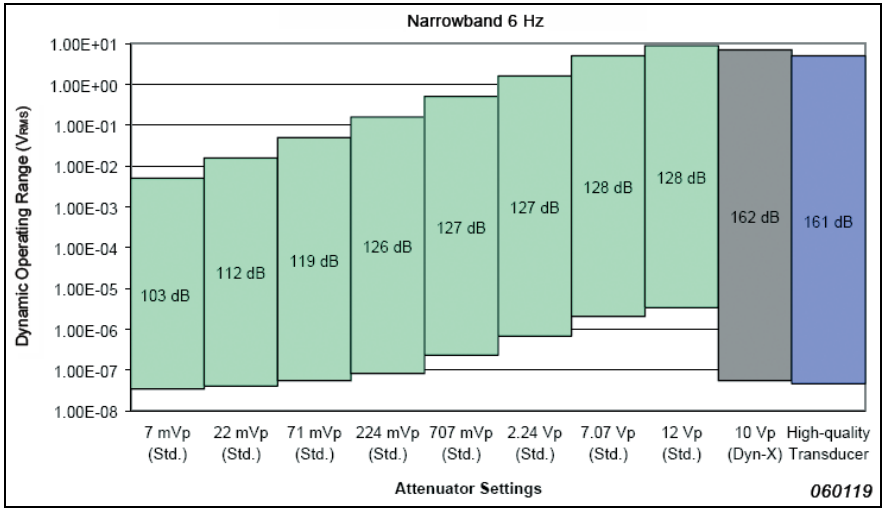

Fig. 4 and Fig. 5 compare the dynamic performance of a standard high-quality 24-bit input channel with the new Dyn-X input channel. In Fig. 4, a 25.6 kHz bandwidth is used.

In Fig. 5, a 6 Hz bandwidth is used – corresponding to what would be achieved using a 25.6 kHz FFT analysis, with 6400 lines and Hanning weighting.It can be seen that the Dyn-X input channel covers practically the same range as the 8 input attenuator settings of the standard 24-bit input channel and that the dynamic operating range of the Dyn-X input channel matches that of a high-quality transducer. The dynamic ranges are calculated using guaranteed noise levels.

Dyn-X Technology System Performance

It has previously been mentioned that the whole chain must have a dynamic operating range better than 124 dB for a 25.6 kHz broadband analysis, and correspondingly better than 160 dB for a 6 Hz narrowband analysis, in order to match the specifications of high-quality transducers. The following examples compare the performance of the Dyn-X input channel to a standard 24-bit input channel. Note that the standard channel when set to a lower input range can, in theory, provide measurements of similar quality, but with a high risk of generating overloads. The maximum input is $7\,V_{RMS}$ ($10\,V_{peak}$) for the Dyn-X input channel and $5\,V_{RMS}$ ($7\,V_{peak}$) for the standard 24-bit input channel.

In Fig. 6 (left) the two channels are compared for a 1 kHz sine wave attenuated 60 dB (re. 7 V) corresponding to a signal level of $7\,mV_{RMS}$. FFT analysis in 25.6 kHz, 6400 lines and Hanning weighting was used resulting in an effective noise bandwidth of 6 Hz. For the Dyn-X input channel noise and spurious components are below –160 dB, thus matching the performance of high-quality transducers. The noise floor of the standard 24-bit input channel is approx. 30 dB higher and distortion components are clearly visible indicating non-linearity in the ADC.

In Fig. 6 (right), a similar comparison is done, but now with the sine wave attenuated 150 dB (re. 7 V) corresponding to a signal level of $0.22\,\mu V_{RMS}$. The noise floor and the spurious components are below –160 dB for the Dyn-X input channel and the sine wave is easily detected. For the standard 24-bit input channel, the sine wave is buried in noise. Noise and distortion components from ADC non-linearity are clearly visible in the standard channel.

In Fig. 7 the two channels are compared in the time domain for a 1 kHz sine wave attenuated 90 dB (re. 7 V) corresponding to a signal level of $0.22\,mV_{RMS}$. Again noise and distortion components are clearly visible in the standard 24-bit input channel.

Fig. 6. Comparison of Dyn-X input channel and standard 24-bit input channel. Left: –60 dB (7 mV$_{RMS}$) 1 kHz sine wave. Right: –150 dB (0.22 μV$_{RMS}$) 1 kHz sine wave

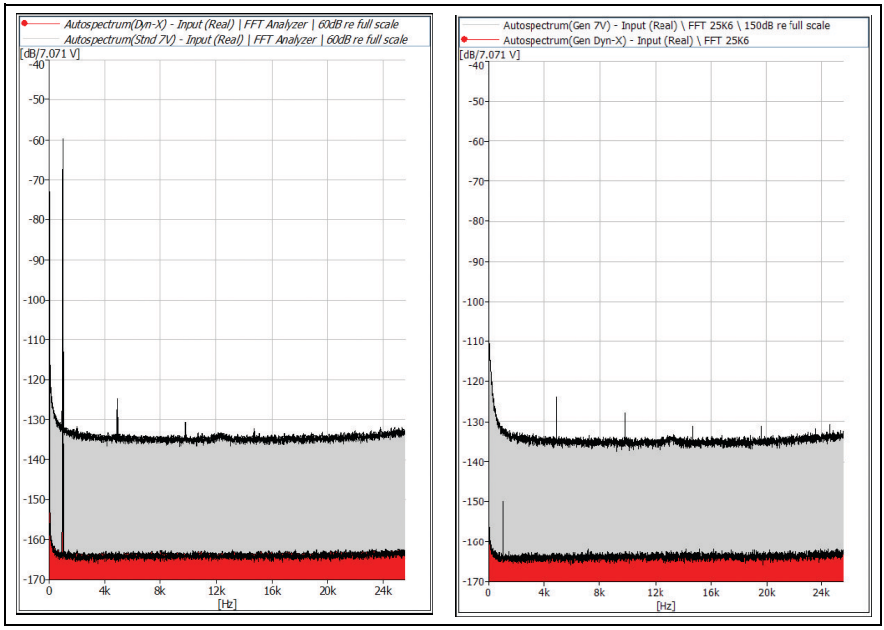

Fig. 7. Comparison of Dyn-X input channel and standard 24-bit input channel for a –90 dB (0.22 mV$_{RMS}$) 1 kHz sine wave

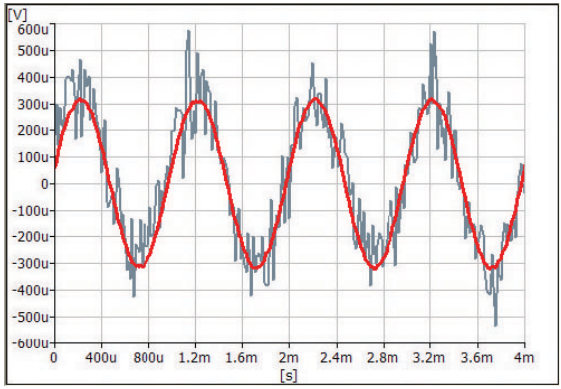

In Fig. 8, a microphone measurement example is shown. The measurement is performed in a standard office environment with background speech and a person whistling. FFT analysis is used in 25.6 kHz with 1600 lines giving a frequency resolution of 16 Hz. The microphone signal is measured by both channels in parallel.

Fig. 8. Comparison of Dyn-X input channel and standard 24-bit input channel. Microphone measurement in office

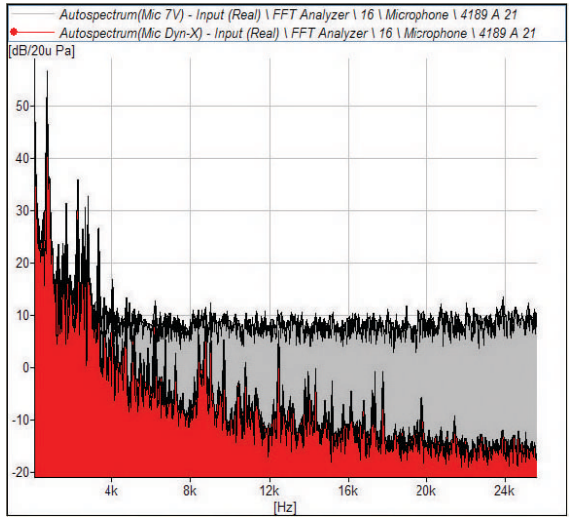

This simple measurement clearly illustrates the improved dynamics of the Dyn-X input channel when compared to the standard 24-bit input channel. The difference is close to 30 dB above 4 kHz. The standard 24-bit input channel measures system noise instead of environmental office noise.

Benefits

With no setting of input ranges, and with no need to be concerned about overloads, under-range measurements and the accuracy of the measurements obtained, the ease and safety of performing sound and vibration measurements are dramatically increased using Dyn-X input modules. And with no need for trial runs to ensure correct input ranges for the various input channels, the certainty of getting the measurements right the first time is also significantly increased.

Dyn-X is a technology that can be usefully employed in a number of measurement situations and applications as shown in Table 5. Using a standard input module with input attenuators would in most cases, be impractical, and in some cases, even impossible.

Table 5. Examples where the Dyn-X technology can be usefully employed

<table>
<tr><td>When the measurement must be right the first time
• Crash testing
• Destructive testing
• Heavy Machinery – run up/coast down</td><td rowspan="2">When signal levels are unknown
• Run up/down
• Field testing
• Trouble shooting</td></tr>
<tr><td>When time is limited
• Test cells
• Wind tunnels
• Road testing
• Flight testing</td></tr>
<tr><td>When user interaction is minimal
• Road testing
• Flight testing
• Untrained operator</td><td rowspan="2">When it is difficult to get an overview of the whole measurement scenario
• Multi-channel measurements
• Multi-analysis measurements
• Test cells
• In-car testing
• Sound, vibration and other parameters involved</td></tr>
<tr><td>When testing is unattended
• Monitoring
• Production line testing</td></tr>
</table>

Conclusions

For the last 30 to 40 years, high-quality transducers have outperformed analysis systems with respect to linearity and dynamic performance. Several weak links in the analysis chain have reduced the resulting analysis performance and an input attenuator has been required to accommodate the dynamic range of the transducer. This increases the risk of overload and under-range situations and it forces the user to constantly pay attention to the measurement status.

24-bit ADCs are today industry standard and are in theory able to handle the full dynamic range of high-quality transducers without the inclusion of an input attenuator.

However, until now, no commercial ADCs have had sufficient performance to allow for elimination of the input attenuator.

With the introduction of the innovative Dyn-X technology, significant performance increase has been achieved in both the analog conditioning and the digital signal processing. As demonstrated with measurement examples, the Dyn-X technology matches the high dynamic performance of high-quality transducers, thereby totally eliminating the need for input attenuators. Consequently, measurements become safer, a higher measurement quality can be achieved and the operator does not constantly have to pay attention to the actual signal levels to avoid overload and underrange situations.

References

[1] Randall R.B., "*Frequency Analysis*", Brüel & Kjær, 3rd edition, 1987.

[2] Clayton G.B., "*Data Converters*", MacMillan Publishers, 1st edition, 1982.

Order Tracking in Vibro-acoustic Measurements: A Novel Approach Eliminating the Tacho Probe

Thorkild Find Pedersen, Svend Gade, Henrik Herlufsen, Hans Konstantin-Hansen

Abstract

Access to the rotating parts of machinery can at times be difficult, or even impossible, so mounting of tacho-probes for measurement of the rotational speed of the shaft and its harmonics is a challenge. To overcome this problem a new order tracking method has been developed, where the fundamental frequency is extracted from the measured vibration and/or acoustic signals, thus making the need for a tacho-probe superfluous. Furthermore, the amplitude and phase of specified orders can also be estimated. The technique is based on Bayesian statistics, where the posterior distribution of the fundamental frequency conditioned on the measured data and a harmonic model of the signal is computed. To validate this technique it was tested using the vibration signals from the drive train of a passenger car and compared with two other order tracking methods: resampling based order tracking, and; the Vold-Kalman tracking filter.

Résumé

Il est quelquefois difficile, voire impossible, d'avoir accès aux éléments tournants de certaines machines pour y placer les sondes tachymétriques qui permettent de mesurer les vitesses de rotation des arbres et leurs harmoniques. Pour contourner l'obstacle, une méthode a été mise au point, qui consiste à extraire la fréquence fondamentale des signaux acoustiques et/ou vibratoires mesurés, et rend ainsi superflu l'utilisation de sondes tachymétriques. Les valeurs d'amplitude et de phase d'ordres sélectionnés peuvent aussi être calculées. Cette approche est basée sur les méthodes bayésiennes en analyse statistique, avec calcul de la distribution postérieure de la fréquence fondamentale, conditionnée par les valeurs mesurées, et calcul d'un modèle harmonique du signal. Cette méthode est testée sur les si-gnaux vibratoires émis par le train de transmission d'un véhicule automobile et comparée

à deux autres méthodes de tracking: suivi d'ordres par rééchantillonnage, et suivi d'ordres par filtrage Vold-Kalman.

Zusammenfassung

Rotierende Maschinenteile können zuweilen schwer oder überhaupt nicht zugänglich sein. Die Montage von Tachogebern für die Messung der Wellendrehzahl und ihrer Harmonischen stellt damit eine Herausforderung dar. Um dieses Problem zu überwinden, wurde ein neues Ordnungsanalyseverfahren entwickelt, bei dem die Grundfrequenz aus dem gemessenen akustischen oder Schwingungssignal extrahiert wird, wodurch der Tachogeber überflüssig wird. Außerdem lassen sich Amplitude und Phase bestimmter Ordnungen abschätzen. Die Technik beruht auf Bayesian-Statistik, wobei die posteriore Verteilung der Grundfrequenz aus den aufbereiteten Messwerten und einem harmonischen Signalmodell berechnet wird. Zur Validierung der Methode wurde sie an Schwingungssignalen vom Antriebsstrang eines PKWs überprüft und mit zwei anderen Ordnungsanalyseverfahren verglichen: Ordnungsanalyse mit Resampling und Vold-Kalman-Filterung.

Introduction

Detection of periodic components in noisy signals is a problem of considerable theoretical interest and great practical importance. Here we apply the standard Bayesian approach of periodic component detection to a non-stationary measurement from a normal passenger car. Our objective is to derive a simple and reliable RPM estimator for rotating machines.

The fundamental frequency is typically measured using dedicated sensors like proximity probes or photo sensors requiring direct access to the rotating parts of the machine. Often rotating parts are not easily accessible and, even if they are, then mounting and setting up the tacho probe is a problem in itself. It is therefore of interest to investigate the possibility of extracting the fundamental frequency from other sources, for instance, the sound and vibration signals already measured for other analysis purposes.

In the following section, Bayesian spectral estimation theory [1, 3] is reviewed. The objective of this analysis is to compute the posterior probability of the event that the fundamental frequency is ω_0, for example, the conditional probability $p(\omega_0,|\mathbf{d}, I)$ where I represents the prior knowledge in the estimation model, and $\mathbf{d}$ represents the measured signal. In order to cope with non-stationary signals, we segment the signal into overlapping records and compute the posterior probability

for each record. By introducing a prior on ω_0 conditioned on the previous L records, the estimator is further extended to include tracking of smooth changes in the fundamental frequency, for example, $p(\omega_0^{(l)}|\mathbf{d}, I) = p(\omega_0^{(l)}| \omega_0^{(l-1)}, \omega_0^{(l-2)}, ..., \omega_0^{(l-L)}, \mathbf{d}, I)$, where superscript l is the time index of the current record. The extension, which allows the estimation of amplitudes and phases of specified orders of the fundamental frequency, is described in the subsequent sections. The method is tested using a vibration signal measured by an accelerometer mounted on the drivetrain of a passenger car. A second measurement is also taken using an accelerometer mounted on a small turbo-charger.

Bayesian Estimation and Tracking

The motivation for using the Bayesian statistical framework to estimate the fundamental frequency is that it allows for simple inclusion of prior knowledge in the estimation process. The impulsive nature of rotating and reciprocating machines results in the presence of higher harmonics of the fundamental frequency in the observed signals. For instance, it is well known that the dominant harmonic orders for a 4-cylinder engine is the sequence $K = \{2, 4, \ldots\}$ and for a 6-cylinder engine $K = \{3, 6, \ldots\}$. Within the Bayesian framework this prior knowledge is easily included to improve the performance of the estimator. Another type of prior knowledge that can be included is the rate of change in the running speed.

In the signal processing literature, the problem of detecting and tracking periodic signals is often defined as estimating the amplitude and phase of a number of harmonic components [4], for example:

$$d(t) = a_0 + \left[\sum_{k=1}^{K} a_k \cos(\omega_k t) + b_k \sin(\omega_k t) \right] + e(t) \qquad (1)$$

The noise-term $e(t)$ is assumed zero mean, white and Gaussian with variance, σ^2. The frequencies in the harmonic sequence are defined as orders α_k of the fundamental frequency, ω_0, for example, $\omega_k = \alpha_k \omega_0$.

For a segment of samples, equation (1) can be reformulated as the linear problem:

$$\mathbf{d} = \mathbf{G}\mathbf{b} + \mathbf{e} \qquad (2)$$

where the column vector **d** is the observed or measured data, **G** is a matrix with basis vectors as columns corresponding to the sines and cosines, **b** is a column vector with the associated amplitudes and **e** is the noise contribution:

$$\begin{aligned}
\mathbf{d} &= [d(t_0), \ldots, d(t_{N-1})]^\top \\
\mathbf{G} &= [\mathbf{1}, \cos(\mathbf{t} \cdot \mathbf{\Omega}^\top), \sin(\mathbf{t} \cdot \mathbf{\Omega}^\top)] \\
\mathbf{b} &= [\alpha_0, \ldots, \alpha_K, b_1, \ldots, b_K]^\top \\
\mathbf{t} &= [t_0, \ldots, t_{N-1}]^\top \\
\mathbf{\Omega} &= [\omega_1, \ldots, \omega_K]^\top
\end{aligned} \tag{3}$$

Estimation

Bayes theorem states that the joint posterior probability density function (PDF) of the parameters in a model, equals the likelihood of the data multiplied by the prior knowledge of the parameters, divided by the evidence of the data. Mathematically this is expressed as:

$$p(\Theta|\mathbf{d}) = \frac{p(\mathbf{d}|\Theta)p(\Theta)}{p(\mathbf{d})}$$

where Θ and **d** respectively represents the model parameters and the data.

Using Bayes theorem the posterior distribution of ω_0 conditioned on the measurement data is given by:

$$p(\omega_0, \{\sigma, \mathbf{b}\}|\mathbf{d}) = \frac{p(\mathbf{d}|\omega_0, \{\sigma, \mathbf{b}\})p(\omega_0, \{\sigma, \mathbf{b}\})}{p(\mathbf{d})} \tag{4}$$

To find the distribution of the observations conditioned only on ω_0, the nuisance parameters, $\{\sigma, \mathbf{b}\}$, must be eliminated by marginalisation of the likelihood $p(\mathbf{d}|\omega_0, \{\sigma, \mathbf{b}\})$ which simplifies equation (4) into [1]:

$$p(\omega_0|\mathbf{d}) \propto p(\mathbf{d}|\omega_0)p(\omega_0) \tag{5}$$

The marginalisation of the likelihood depends on the prior distribution chosen for the nuisance parameters. In [1, 3] an analytical solution is derived when the amplitudes are assigned uniform priors, $p(\mathbf{b}_m)$ = const, and Jeffrey's prior [2] is used for the noise variance, $p(\sigma_m) = \text{const}/\sigma_m$:

$$p(\mathbf{d}_m \mid \omega_0) \propto \frac{\left(\mathbf{d}^\top\mathbf{d} - \mathbf{d}^\top\mathbf{G}(\mathbf{G}^\top\mathbf{G})^{-1}\mathbf{G}^\top\mathbf{d}\right)^{\frac{-(N-2K-1)}{2}}}{\sqrt{|\mathbf{G}^\top\mathbf{G}|}} \tag{6}$$

Tracking

The linear model in equation (2) assumes a stationary signal. To release this assumption and allow tracking of smooth changes in ω_0, the measured signal is segmented into L overlapping records of suitable lengths, and ω_0 is assumed approximately constant in a given record.

A computationally tractable prior on the changes of the fundamental frequency is obtained by letting the process be random with a Gaussian first derivative. This is shown in equation (7) where ${\omega_0}^{(l)}$ denotes the fundamental frequency of the l^{th} record:

$$\omega_0^{(l)} - \omega_0^{(l-1)} = \omega_0^{(l-1)} - \omega_0^{(l-2)} + \mathcal{N}(0, \sigma_T^2) \tag{7}$$

The prior distribution for ω_0 can then be expressed as:

$$p(\omega_0^{(l)} \mid \omega_0^{(l-1)}, \omega_0^{(l-2)}) = \frac{1}{\sqrt{2\pi{\sigma_T}^2}} \exp \frac{-(\omega_0^{(l)} + 2\omega_0^{(l-1)} - \omega_0^{(l-2)})^2}{2{\sigma_T}^2} \tag{8}$$

The posterior distribution for each record, l, is then given by inserting equations (6) and (8) into equation (4). This particular choice of tracking prior amounts to choosing $L = 2$

The profile of the fundamental frequency is now found as the set of ${\omega_0}^{(i)}$ which maximizes the posterior of the individual records, $p({\omega_0}^{(i)} \mid \mathbf{d}^{(i)})$:

$$\left\{ \arg\max_{\omega_0^{(i)}} p(\omega_0^{(i)} \left| \mathbf{d}^{(i)}) : 0 \le i < M \right. \right\} \tag{9}$$

(assuming a total of M records)

Non-stationary Amplitude Estimation

In traditional resampling based order-tracking the measured signals are resampled from having a time varying frequency in the time domain to having a constant frequency in the angular domain. With stationary frequencies, the complex amplitudes of the harmonic orders are estimated with the Fourier transformation. The method proposed here modifies the set of basis functions in **G** to reflect changes in the fundamental frequency, instead of resampling the measured signals. The definition of **G** in equation (3) then becomes:

$$\mathbf{G} = [\mathbf{1}\ \mathrm{gc}_1(\mathbf{t}) \ldots \mathrm{gc}_K(\mathbf{t})\ \mathrm{gs}_1(\mathbf{t}) \ldots \mathrm{gs}_K(\mathbf{t})] \tag{10}$$

where the functions for computing the basis vectors are defined by:

$$\mathrm{gc}_k(\mathbf{t}) \equiv \cos(\alpha_k\ \Omega_F(t)), \qquad \mathrm{gs}_k(\mathbf{t}) \equiv \sin(\alpha_k\ \Omega_F(t)) \tag{11}$$

$$\Omega_F(t) = \int_0^t \omega_0(\tau) d\tau \tag{12}$$

Knowing the fundamental frequency and orders of interest, **G** can be formed. The corresponding amplitudes are then found by solving the linear problem of equation (2). The least mean square error solution to this is:

$$\mathbf{b} = (\mathbf{G}^\top \mathbf{G})^{-1} \mathbf{G}^\top \mathbf{d} \tag{13}$$

If the fundamental frequency is estimated for overlapping segments of the data, then interpolation is used to compute the frequency value for the intermediate

samples. The basis functions in **G** are then formed according to equations (10), (11) and (12).

To compare the estimates with re-sample based order analysis, the length of each segment is adjusted to span the same number of periods of the fundamental frequency. This is also true for the overlaps between segments.

Experimental Validation

Both the frequency tracker and amplitude estimator are tested on vibration data from a drivetrain. Fig. 1 shows the accelerometer mounted close to a bearing on the drivetrain. The drivetrain is mounted on a test bench and powered by an electric motor. The speed can be controlled manually or set to one of four fixed operating speeds: 1140 RPM, 2900 RPM, 4300 RPM, or 4990 RPM.

Fig. 1. Experimental Setup – The picture shows the mounting position of the accelerometer and tacho probe on the drivetrain

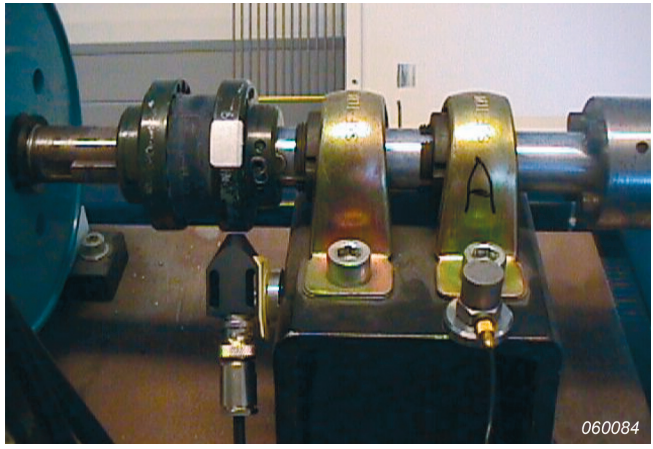

In this experiment, the measurement starts at the lowest speed and runs for approximately 10 seconds at each of the fixed speeds, after which the speed is reduced manually over the last 20 seconds of the run, totaling (approximately) a 60 second measurement.

RPM Estimation

The time-varying frequency content of the vibration signal is shown in Fig. 2. The fundamental frequency is observed to be in the range $0 < \omega_0/2\pi < 100$ Hz. It therefore suffices with a 400 Hz bandwidth corresponding to a sample rate of Fs = 1024 Hz. The first four harmonics are clearly visible in the spectrogram. Therefore, the posterior distribution of ω_0 is computed for the harmonic sequence K = {1, 2, 3, 4}.

To obtain a satisfactory time resolution, the vibration signal is segmented into records of 1/4 second, overlapping 75%. The resulting posterior distribution is shown on a logarithmic scale in Fig. 3.

Fig. 2. Experimental Data – Spectrogram of the measured acceleration signal. Each record is 0.25 seconds long and Hanning weighted. Overlap is set to 50%

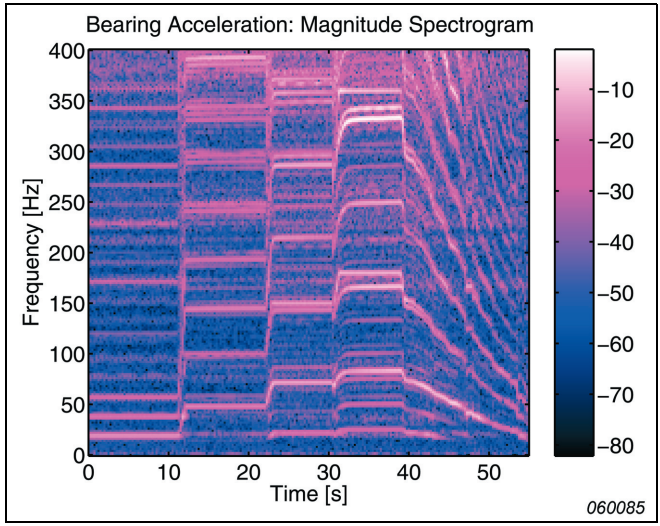

Initializing the prior defined in equation (8) with $\sigma_T^2 = 0.5$ results in the track shown in Fig. 4. The tracked frequency is plotted on top of the true RPM profile measured with an optical tacho probe at full measurement bandwidth. The difference is hardly visible. This is confirmed in Fig. 5 where the difference of the two is plotted.

The error is most noticeable when the speed changes rapidly. In the stationary intervals the error stays within ±3 RPM.

Fig. 3. Posterior distribution of the fundamental frequency for the harmonic sequence K = {1, 2, 3, 4}

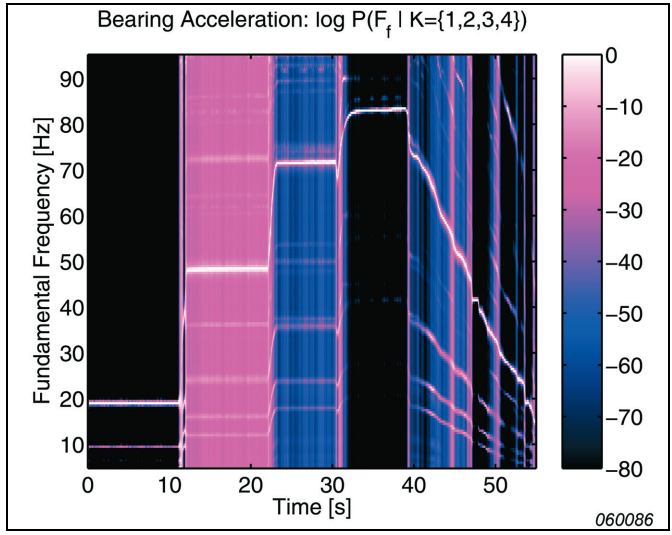

Fig. 4. RPM Profile

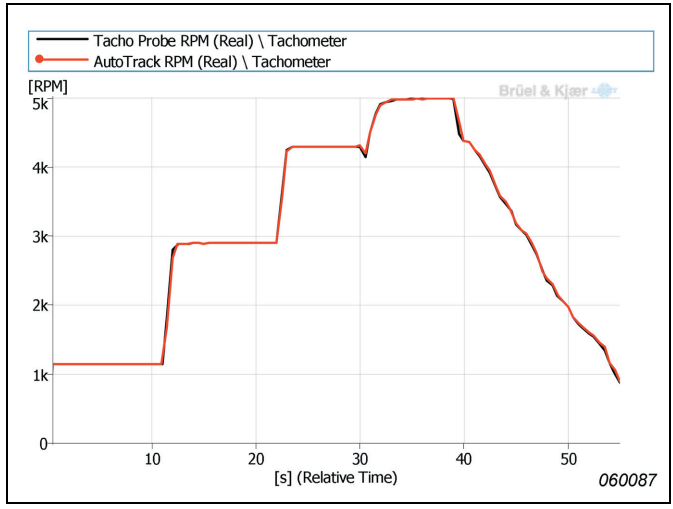

Fig. 5. RPM Estimation Error

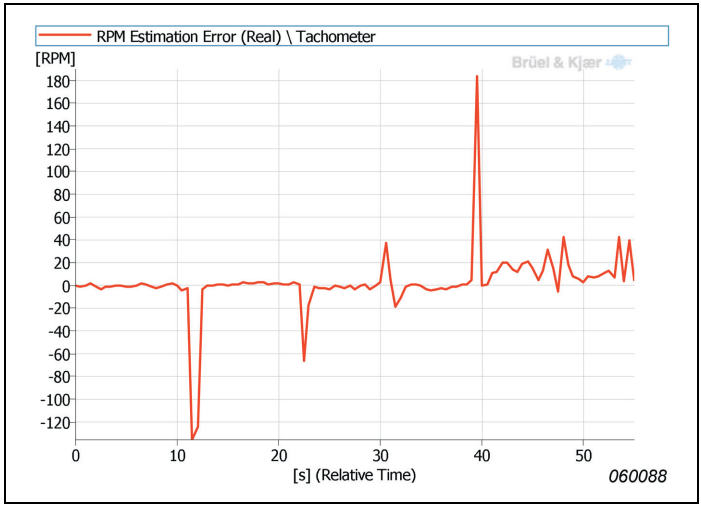

Amplitude Estimation

For amplitude estimation the record length is set to 20 periods of the fundamental frequency and the overlap to 15 periods. This is equivalent to a Brüel & Kjær Type 7702 Order Analyzer configured to a span of 5 orders, with a resolution of 100 lines and 75% overlap.

The fundamental frequency for each sample is computed with cubic spline interpolation of the frequency profile shown in Fig. 4. It is used to estimate the amplitudes of the first four harmonic orders.

For comparison, the same harmonic orders are estimated using both a 2nd order Vold-Kalman filter [5] and an Order Analyzer, as described above.

The result for the first harmonic order is shown in Fig. 6 and for the second harmonic in Fig. 7. For both harmonics the new estimator produces comparable results to the Order analyzer. However, for the second harmonic, the new estimator matches the Vold-Kalman estimates better than the Order analyzer.

Fig. 6. First Harmonic

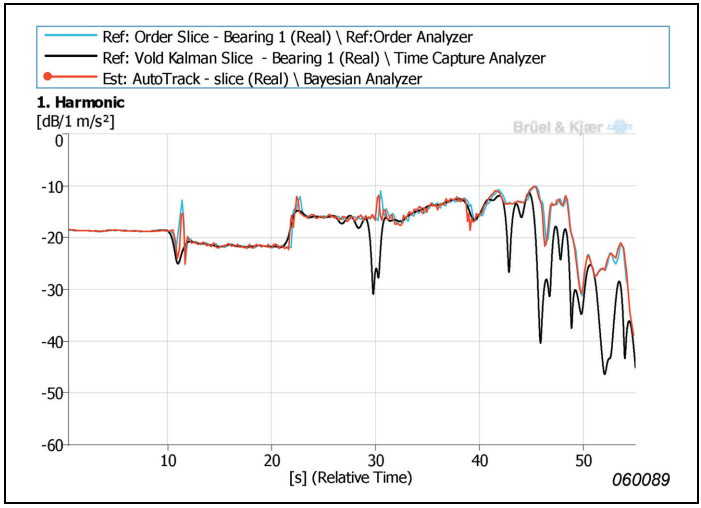

Fig. 7. Second Harmonic

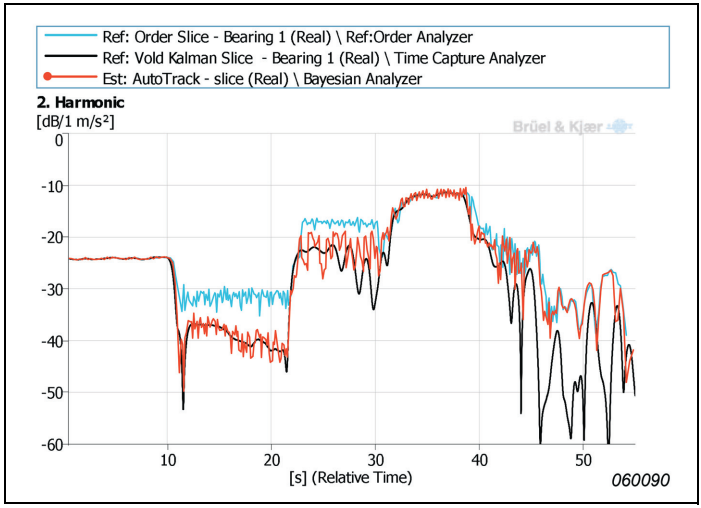

Turbo-charger

The last example in this paper is the vibration signal from an accelerometer mounted on a small turbo-charger. The spectrogram of the signal is shown in Fig. 8, where two distinct profiles are visible. One is at low frequencies with many higher harmonic orders. This is the fundamental frequency of the engine. The other profile at high frequencies (3 kHz) is the first order of the turbo-charger.

Fig. 8. Turbo-charger spectrogram

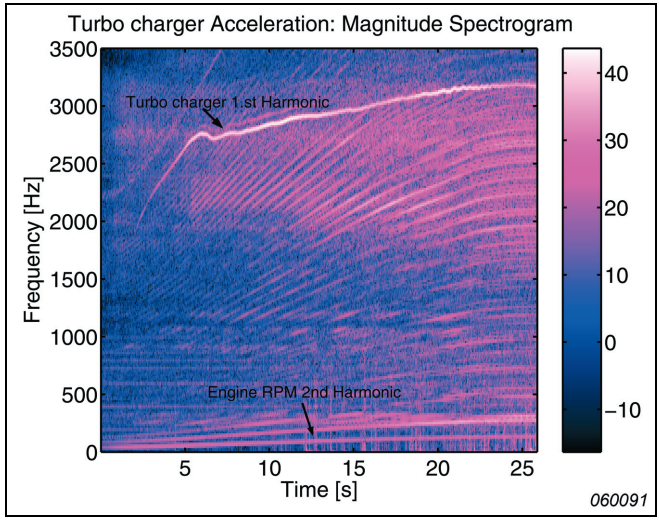

For a successful tracking of the turbo-charger RPM, it is necessary to use short segments. Experimentally it was found that a fixed length of T=1/16s was sufficient, combined with the harmonic model $K = \{1\}$ and a tracking variance of $\sigma_T^2 = 150$. No reference is available for validation but the profile shown in Fig. 9 matches the visible line in Fig. 8.

The engine RPM was extracted successfully from the same signal, using the same parameter that was used for the drive train – the only difference between them was the harmonic sequence $K = \{2, 4\}$, which represented the two dominant orders of the 4 cylinder engine (results not shown).

Fig. 9. Estimated RPM of turbo-charger

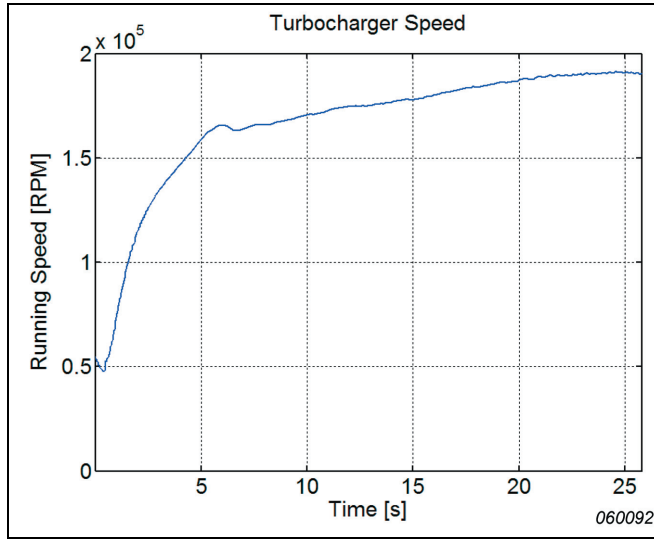

Discussion and Conclusions

The Bayesian paradigm has proven useful in devising a method to estimate and track the fundamental frequency of a rotating machine.

The viability of the method was demonstrated using real data. Experimental data showed the method's usefulness in solving the practical problem of determining the running speed of the engine in a passenger car. Not only was the method capable of providing accurate estimates, but it was also able to track fast slew rates in the excess of 1000 RPM per second. Even a turbo-charger's RPM could be estimated.

A novel technique was demonstrated for computing the complex amplitudes of individual harmonic orders. This was accomplished by re-sampling the basis functions instead of the measured time domain data. In situations where only a few orders are to be estimated – or the channel count is high – this approach may prove computationally more efficient compared to conventional order analyzers.

There are further issues to be addressed. Choosing the right tracking prior parameter is an open problem, which we will address using a learning algorithm à la Baum- Welch [6]. Choosing the most appropriate harmonic sequence for the spectrum estimator is another important issue.

References

[1] Joseph J.K. Ò Ruanaidh and William J. Fitzgerald, "*Numerical Bayesian Methods Applied to Signal Processing*", Statistics and Computing, Springer, 1998.

[2] H. Jeffreys, "*Theory of Probability*", Oxford University Press, London, 1939.

[3] G. L. Bretthorst, "*Bayesian Spectrum Analysis and Parameter Estimation*", vol. 48 of Lecture Notes in Statistics, Springer-Verlag, 1988.

[4] A. Nehorai and B. Porat, "*Adaptive Comb Filtering for Harmonic Signal Enhancement"*, IEEE Transactions on Acoustics, Speech and Signal Processing, vol. ASSP-34, no. 5, pp. 1124-38, 1986.

[5] S. Gade, H. Herlufsen, H. Konstantin-Hansen and H. Vold, "*Characteristics of the Vold-Kalman Order Tracking Filter*", Brüel & Kjær Technical Review No. 1 – 1999.

[6] L. R. Rabiner, "*A tutorial on hidden Markov models and selected applications in speech recognition"*, Proceedings of the IEEE, 77(2): 257–286, February 1989.

Comparison of Acoustic Holography Methods for Surface Velocity Determination on a Vibrating Panel

Niels-Jørgen Jacobsen, J. Mørkholt, A. Schuhmacher

Nomenclature

p	Sound Pressure
v_n	Normal Velocity
ω	Angular Frequency
ρ	Fluid or Material Density
$G(P,Q)$	Green's Function
H	Transfer Function
$\mathcal{F}$	Spatial Fourier Transform
$G(k_x,k_y,z)$	Inverse Propagator Kernel
f_d	Doppler Frequency
λ	Wavelength of Laser Beam
f_c	Eigenfrequency
c	Speed of Sound
D	Bending Stiffness
E	Young's Modulus
υ	Poisson's Ratio

Abstract

Two different acoustic holography methods for surface velocity determination are compared by experiment: Inverse Boundary Element Method (IBEM) and Planar Near-field Acoustical Holography (PNAH). While IBEM enables the estimation of surface velocity on arbitrary geometries, the PNAH method provides velocity estimates in a plane close to the structure under investigation. Both methods make use of acoustic near-field measurements. The results of the acoustic holography methods are compared to the results obtained directly from measurements on a vibrating panel using a Laser Doppler Vibrometer (LDV).

Résumé

Deux différentes méthodes d'imagerie par holographie acoustique pour la détermination d'une vitesse de surface sont comparées aux fins d'expérimentation: une méthode par éléments de frontière désignée IBEM (Inverse Boundary Element Method) et une méthode par holographie acoustique de champ proche de type planaire désignée PNAH (Planar Near-field Acoustical Holography). La méthode IBEM permet des estimations de vitesse de surface sur des géométries arbitraires, tandis que la méthode PNAH fournit des estimations de vitesse dans un plan proche de la structure testée. Les résultats obtenus au moyen de ces deux méthodes sont comparés aux mesures prises directement sur une surface vibrante à l'aide d'un vibromètre laser à effet Doppler.

Zusammenfassung

Zwei verschiedene akustische Holographieverfahren zur Ermittlung der Oberflächengeschwindigkeit werden experimentell miteinander verglichen: Indirekte Boundary-Elemente-Methode (IBEM) und planare akustische Nahfeldholographie (PNAH). Während IBEM die Abschätzung der Oberflächengeschwindigkeit auf beliebigen Geometrien ermöglicht, liefert die PNAH-Methode Geschwindigkeitsabschätzungen in einer Ebene in unmittelbarer Nähe der untersuchten Struktur. Beide Verfahren verwenden akustische Nahfeldholographie. Die Ergebnisse der akustischen Holographieverfahren werden mit direkten Messergebnissen verglichen, die mit einem Laser-Doppler-Vibrometer (LDV) an einer vibrierenden Platte erhalten wurden.

Introduction

Non-contact measurement techniques for vibration analysis have the advantage compared to more traditional transducer mounting methods that they totally eliminate mass loading and thereby do not change the structure's inherent dynamics. Furthermore, they permit measurements to be performed under demanding conditions, for example, measuring on surfaces with high temperatures. As the different techniques have different unique advantages, non-contact measurement techniques are not 'just' used for applications where traditional contact transducers are inapplicable, but also as a fast alternative to traditional contact measurement techniques

In this paper, three different non-contact techniques are compared: IBEM, PNAH and Single-point LDV. As LDV is a well-established and accurate vibration measurement technique, this method serves here as a reference method for determining the validity of velocity distributions and absolute levels obtained by the IBEM and PNAH methods.

IBEM has previously been compared to the Scanning LDV method using a loudspeaker as measurement object [1] and to the LDV method using a vibrating panel as measurement object [2]. This paper is a further development of the latter by including PNAH, by using a complete LDV scanning of the measurement surface for comparison and by further investigation of the differences between the techniques.

Theory – Inverse Boundary Element Method

The Inverse Boundary Element Method (IBEM), based upon the boundary element method (BEM) in acoustics [3], is one of the most interesting, novel, non-contact vibration measurement techniques. The idea behind BEM is the possibility of expressing the sound pressure at a given location, exterior to a radiating structure, in terms of variables – usually sound pressure and normal velocity – defined on an arbitrary surface, Fig. 1. In that way the 3D sound field outside a radiating structure can be simulated if sound pressure and normal velocity are known on the structure itself, for example, on a surface in 3D space.

Fig. 1. Structure with boundary surface S located in a fluid. P is an observation point in the fluid at distance R from an integration point Q on S

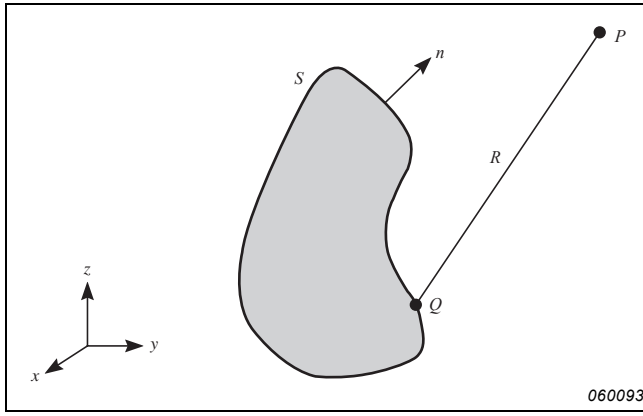

In mathematical terms, this relationship can be expressed as the Helmholtz integral equation:

$$p_f(P) = \int_S (p(Q)\partial G(P, Q)/\partial n + j\omega\rho v_n(Q)G(P, Q))dS(Q) \quad (1)$$

where P and Q are a field point and a surface point respectively, p denotes sound pressure, v_n is normal velocity and G is the Green's function:

$$G(P, Q) = e^{-jkR}/4\pi R, \quad R = |P - Q| \quad (2)$$

In order to make use of the Helmholtz integral equation, we must know both the sound pressure and the normal velocity on the surface *S* before we can compute the sound pressure at a field point *P*. However, in many cases, only the normal velocity is known, so in this case we must solve for the unknown sound pressure on *S* before using equation (1). In practice, a surface mesh of the boundary surface is made by a number of interconnected elements, for example, triangles or squares, and equation (1) can be written as a linear matrix system with the use of numerical integration. The process described here can be classified as a forward BEM problem.

In contrast to this approach, the IBEM uses acoustic sound field measurements around the structure to reconstruct the surface normal velocity and is based on a numerical model of the acoustic environment surrounding the structure. The numerical model relates the measured sound field around the structure, as represented by a vector of discrete sound pressure sampling points, to the surface normal velocity of the structure as represented by a vector of discrete surface velocity sampling points. These points correspond to the nodes of a surface mesh discretization of the surface of the structure. The model should thus include the structure under test and any other obstacles close to it and in many cases also the hard ground under the structure. The relation between field sound pressures and surface node velocities may be written in matrix-vector form as:

$$\begin{pmatrix} p_1 \\ p_2 \\ \vdots \\ p_i \\ \vdots \\ p_m \end{pmatrix} = \begin{pmatrix} H_{11} & H_{12} & \dots & H_{1j} & \dots & H_{1n} \\ H_{21} & H_{22} & \dots & H_{2j} & \dots & H_{2n} \\ \vdots & \vdots & \ddots & \vdots & \ddots & \vdots \\ H_{i1} & H_{i2} & \dots & H_{ij} & \dots & H_{in} \\ \vdots & \vdots & \ddots & \vdots & \ddots & \vdots \\ H_{m1} & H_{m2} & \dots & H_{mj} & \dots & H_{mn} \end{pmatrix} \begin{pmatrix} v_1 \\ v_2 \\ \vdots \\ v_j \\ \vdots \\ v_n \end{pmatrix} \tag{3}$$

where p_i is the measured sound pressure at the i'th microphone and v_j is the surface normal velocity at the j'th node of the boundary element mesh. The relation between p_i and v_j is established through the transfer function H_{ij} determined numerically by the Boundary Element Method. Note that the linear system of equations is only valid at a single frequency and must therefore be recalculated for different frequencies.

The purpose of the IBEM algorithm is to reconstruct the normal velocity at every node from the measured field sound pressures. This is essentially an inverse problem involving inversion of the transfer function matrix of (3). The matrix inversion is done by imposing some sort of regularisation, since the solution would otherwise become meaningless. This is a consequence of the matrix being almost singular for nearly every case. The physical explanation for this near-singularity is that evanescent source radiation information (radiation components corresponding to fast varying surface velocity components) dies out quickly when radiating from the structure, that is, it doesn't give rise to any pressure field far away from the source. Consequently this information can hardly be measured by the microphones and is therefore difficult to reconstruct especially in the presence of noise. In this case, it is better to avoid some of the evanescent information at the price of a reduced surface velocity resolution. It should, however, be emphasised that it is (in general) desirable to reconstruct as much of the evanescent wave information as possible, since this information is associated with short wavelength surface velocity components. (They are responsible for the source resolution, for example, the possibility to separate close sources on the source surface).

In practice the linear system of equations is most often solved using an approach based on Singular Value Decomposition (SVD) of the matrix of transfer functions followed by a regularisation step, essentially grouping the SVD components into useful and unwanted components. Computing the desired solution, for example,

the structural surface velocity vector, is then done via the set of useful components. Deciding on the number of useful components is, however, not trivial but some methods for automatic detection of this subset can be found [4]. Further details about the IBEM method may be found in [5] and [6].

The numerical sound field model used in IBEM assumes a harmonic, totally coherent sound field as input. In general, this is achieved by deriving a cross spectral sound field description from the measured field sound pressures, based on a number of reference signals representing the uncorrelated or partially correlated radiation mechanisms of the test object under investigation. To deal with partially correlated source mechanisms a principal component decomposition [7] of the sound field is carried out and each component then processed in turn by IBEM. Finally, the individual results are added on a power basis to form the total result. However, when using a single reference it is in principle possible to include phase information in the resulting surface velocity output.

Theory – Planar Near-field Acoustical Holography

Another method for non-contact vibration measurement is the Planar Near-field Acoustical Holography (PNAH) method, sometimes also referred to as Spatial Transformation of Sound Fields (STSF) [7]. This method uses purely acoustic measurements in a plane near the structural surface to reconstruct the surface particle velocity. Reconstruction is only possible in planes parallel to the measurement plane and thus the method is best suited for planar structures. PNAH is based on the fact that in the wavenumber domain, under free-field conditions, calculation of the sound field in a plane $z = z_c$ parallel to the measurement plane $z = z_m$ amounts to multiplication with a simple kernel function. The mathematics behind PNAH may be summarised as:

$$v(x, y, z_c) = \mathcal{F}_x^{-1}\mathcal{F}_y^{-1}\left[\mathcal{F}_x\mathcal{F}_y[p(x, y, z_m)]G(k_x, k_y, z_c - z_m)\right] \tag{4}$$

where $p(x,y,z)$ and $v(x,y,z)$ are the sound pressure and particle velocity in the (x,y)-plane at distance z from the source, $\mathcal{F}_x$ and $\mathcal{F}_y$ denote spatial Fourier transforms in the x- and y-directions respectively and $G(k_x,k_y,z)$ is the inverse propagator kernel. In practice, because PNAH is an inverse problem in the same way as IBEM is, care must be taken when applying the propagator kernel, and some sort of regular-

isation must be applied in order to prevent measurement noise from destroying the reconstruction.

The two-dimensional spatial Fourier transformations may be implemented using FFT which makes PNAH calculation extremely fast even for large arrays. Another practical aspect of PNAH to be taken care of is the windowing effects caused by applying a finite array. Such effects may be dealt with by applying spatial windowing functions to the measured field before the PNAH process. Still, the size of the array must be large enough to cover the full surface of the source (a new *Statistically Optimal* variant of PNAH overcomes this limitation [8]). Finally, spatial aliasing must be avoided by maintaining a spatial sampling distance of at least half the acoustical wavelength at the highest frequency of analysis. As in the case of IBEM, PNAH may be combined with the use of principal components to handle the case of multiple, partially correlated or uncorrelated sources.

At this point it should be noted that while LDVs provide measurements of the actual surface velocity, the IBEM and PNAH methods provide an estimate of the vibration velocity based on acoustic near-field measurements. Only the part of the velocity causing a measurable acoustic signal at the receiver microphones may be reconstructed by the methods. However, when considering structure-borne noise problems such an estimate is indeed relevant. Moreover, the IBEM method provides overall source location on arbitrary geometries, without the need for line-of-sight (the PNAH method is limited to planar geometries). Both methods allow for estimation of acoustic quantities like surface sound pressure and sound intensity.

In addition, since conventional BEM can be used to simulate the radiated sound field if the structural vibration pattern is known, the result of an IBEM analysis provides an acoustic source model that may be used in simulations of acoustic radiation in different environments, or, of the effect on sound radiation of damping parts of the vibrating surface. Similar source modelling may be done via PNAH but again with the limitations of planar geometry.

Theory – Laser Doppler Vibrometry

One of the most well-established and well-proven non-contact measurement techniques is based on Laser Doppler Vibrometers (LDVs), either a Single-point LDV, where one point is measured and the laser sensor head is moved to measure another point, or a Scanning LDV (SLDV), where an internal system of mirrors position the laser beam at specified scan positions without moving the laser sensor head.

The LDV principle is based on interferometry, where a laser beam is divided into an internal reference beam and a measurement beam. The measurement beam is directed onto a vibrating test surface and the back-reflected light recombined with the internal reference beam. When the test surface moves, the path difference between the routes followed by the reference and measurement beams changes, resulting in light-intensity modulation of the recombined beam due to interference between the reference and the measurement beams. The frequency of the intensity modulation, known as the Doppler frequency f_d, is directly proportional to the surface velocity v and the wavelength of the laser λ being 632.8 nm for a Helium-Neon laser:

$$f_d = 2v/\lambda \tag{5}$$

The recombined beam is split into two paths. A quarter-wave plate is used in one of the paths so that the two paths are in quadrature, allowing the direction of motion to be determined. By mixing and demodulating the signals, a voltage output with mean value proportional to the surface velocity is obtained. This output is then fed into an analyzer for frequency analysis.

In addition to the previously mentioned general advantages of using non-contacting measurement techniques, the LDV principle permits measurement of structures containing inaccessible parts, measurement of large or distant structures and measuring in demanding environments such as high-radiation fields, high-voltage areas, clean rooms or wind tunnels. Furthermore, LDVs support higher frequency ranges than traditional contact transducers. The Single-point LDV can be the ideal choice when only a few points have to be measured and an SLDV provides additional benefits such as high spatial resolution and faster and more flexible data acquisition.

Measurement Object

The measurement object was originally designed to simulate the interior of a car cabin for a study of measurement-based modelling of sound sources. It consists of a solid concrete tub of internal dimensions: $0.75\,\text{m} \times 1.70\,\text{m} \times 0.60\,\text{m}$, giving an interior volume of $0.77\,\text{m}^3$. The walls and bottom have a thickness of 0.10 m. The tub is closed by a tightly sealed steel plate of thickness 1 mm and dimensions $0.75\,\text{m} \times 1.70\,\text{m}$. Fig. 2 shows pictures of the test object with and without the top cover steel plate mounted.

Fig. 2. The measurement object with, (left) and without, (right) the steel plate mounted

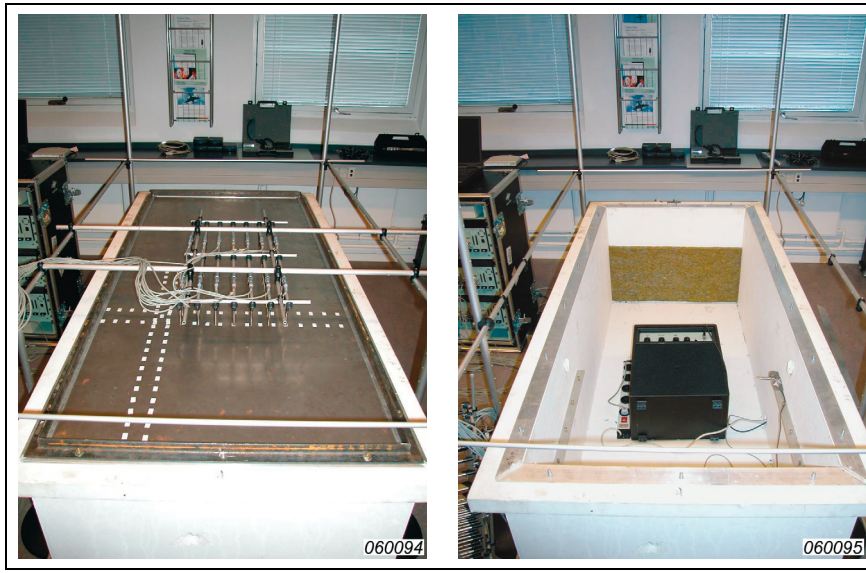

Although the exact boundary conditions of the top cover steel plate are unknown they can be assumed to lie somewhere between clamped and simply supported edges. By assuming simply supported edges one can get an idea of the frequency range of the plate modes. The eigenfrequencies of a simply supported rectangular plate of dimensions a and b and thickness h are given by:

$$f_c = \frac{1}{2\pi}\sqrt{\frac{D}{\rho h}}\left[\left(\frac{m\pi}{a}\right)^2 + \left(\frac{n\pi}{b}\right)^2\right], \qquad m, n = 1, 2\ldots \tag{6}$$

Here D is the bending stiffness of the plate given by $D = Eh^3/12(1-\upsilon^2)$ where E is the Young's modulus and υ is the Poisson's ratio of the plate material, and ρ is the density of the plate material. For steel the material parameters are $E = 2.1 \times 10^{11}$ Nm^{-2}, $\upsilon = 0.31$ and $\rho = 7.8 \times 10^{-3}$ kgm^{-3}. A number of modes and their corresponding eigenfrequencies calculated from the formula are listed in Table 1. Note that only

odd-odd modes are listed since these will be the ones contributing the most to the sound radiation from the plate [9].

Table 1. Frequencies of the plate modes assuming simply supported edges

M	*N*	f_c*(Hz)*	*m*	*n*	f_c*(Hz)*
1	1	5	3	9	109
1	3	12	5	1	110
1	5	26	5	3	117
3	1	40	5	5	131
1	7	46	5	7	151
3	3	47	5	9	179
3	5	61	7	1	216
1	9	74	7	3	223
3	7	81	7	5	236

It follows that below 1 kHz the modal density of the top cover plate is already very high. Moreover, since the plate is quite thin compared to the size of the cavity the acoustic and structural subsystems will be coupled to some degree. All in all these results indicate that the test object is a highly resonant and quite complicated vibro-acoustic system. In the interior of the tub a loudspeaker was placed to excite the steel plate. Only the steel plate was assumed to vibrate. The loudspeaker was fed with a white noise signal having a 10 kHz frequency range. The sound pressure level of the loudspeaker was chosen as a compromise between avoiding non-linear behaviour and excessive background noise at the microphone positions.

IBEM and PNAH – Measurement and Analysis

The setup for the IBEM and PNAH measurements is shown in Figure 3.

A planar array configured with 12×7 Brüel & Kjær Type 4935 microphones was positioned in 12 locations to cover the total surface of the vibrating panel in order to spatially sample the sound field radiated. In total $42 \times 21 = 882$ microphone positions were sampled. In principle, for a general sound source, the sound field on all sides of the source should be sampled in the case of IBEM. However, since the

Fig. 3. The IBEM/PNAH measurement setup (left) and numerical mesh model and field point positions (right)

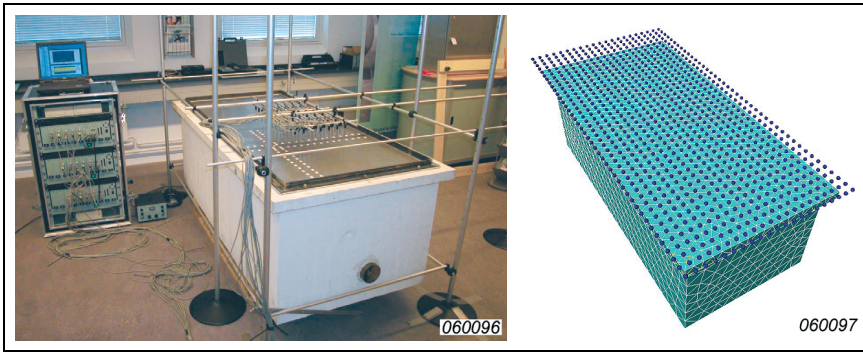

source used was known to radiate mainly from the top cover, it was decided to place microphones on this side only. To avoid spatial aliasing effects the microphone spacing should, as a guideline, be less than half the acoustic wavelength at the maximum analysis frequency. In the present setup the microphone spacing was chosen to be 50 mm, thus corresponding to an upper analysis frequency limit of 3.4 kHz.

The distance to the source was also kept at 50 mm. This distance was chosen as a compromise between ensuring the highest possible surface vibration resolution with the given microphone spacing and at the same time ensuring sufficient decay of very fast spatially varying radiation components, so that the spatial sampling criterion would indeed be fulfilled at the microphone positions [6]. The positions of all field sampling points relative to the test object geometry were also measured, since this information is required for setting up the numerical BEM model relating the surface vibration to the field pressures. Note that the same measurement data was used as input for both the PNAH and IBEM.

Each of the 84 microphones were connected to individual input channels of a Brüel & Kjær Type 3561 Intelligent Data Acquisition (IDA) front-end, which in turn was connected by LAN to a laptop PC running dedicated Brüel & Kjær data acquisition software. All microphones were individually calibrated before measurement. With the loudspeaker source running, simultaneous acquisition from all microphones was done using a sampling rate of 8192 Hz, corresponding to an upper frequency limit of 3.2 kHz. The measurement time was 30 seconds in each scan position. Following the measurement, a cross-spectral sound field description with 3200 lines suitable as input for IBEM was calculated by FFT averaging. The

output from a Brüel & Kjær Type 4935 microphone placed inside the tub, close to the loudspeaker source, was used as reference signal for all scan positions.

A boundary element surface mesh of the measurement object was constructed from a rough sketch but still including the main features of the object. The triangular mesh was designed to a maximum edge length of 45 mm. As a rule of thumb, the edge length should not exceed one quarter of the acoustic wavelength at the maximum analysis frequency [4]. This means that the upper frequency limit for BEM with this mesh was 2 kHz. The resulting mesh consisted of 3444 elements and 1724 nodes as shown in Fig. 3. Note that this figure also shows the microphone positions (marked by dots) relative to the test object geometry.

The PNAH and IBEM calculations were carried out using dedicated Brüel & Kjær software. As stated earlier, in both cases regularisation must be applied when performing the inverse sound field calculations. In this case, a fixed regularisation dynamic range of 40 dB was applied in both instances. This range was found to be adequate based on inspection of results.

Laser Measurement and Analysis

The setup for the LDV measurement is shown in Figure 4. The instrumentation consisted of the Ometron VH300+ Laser Doppler Vibrometer Type 8329, the Portable PULSE™ Type 3560-B front-end and a laptop PC running dedicated PULSE data acquisition and analysis software. The LDV was mounted on a tripod that was positioned on a wooden frame with four soft rubber feet. This arrangement eliminated vibrations being transferred to the LDV and ensured that the laser beam was practically perpendicular to the panel surface at all measurement points. No cosine corrections needed to be applied. The precise distance between the LDV and the panel was not critical but was held at approximately 0.945 m corresponding to one of the optimum working distances. The resulting focus depth was approximately 11 mm.

A rectangular mesh consisting of 462 points (14×33) and with a resolution of 50 mm in both directions was created to cover the plate surface. The measurements were performed directly on the steel surface without dithering – a technique whereby the laser beam is moved to a nearby position until sufficient light is reflected to optimize the signal-to-noise ratio – or treatment of the panel's surface (paint, powder, reflective tape, etc.) to enhance reflectivity. FFT analysis up to 3.2 kHz, 3200 frequency lines and with 50 averages per mesh point was performed.

Fig. 4. The setup for the LDV measurement

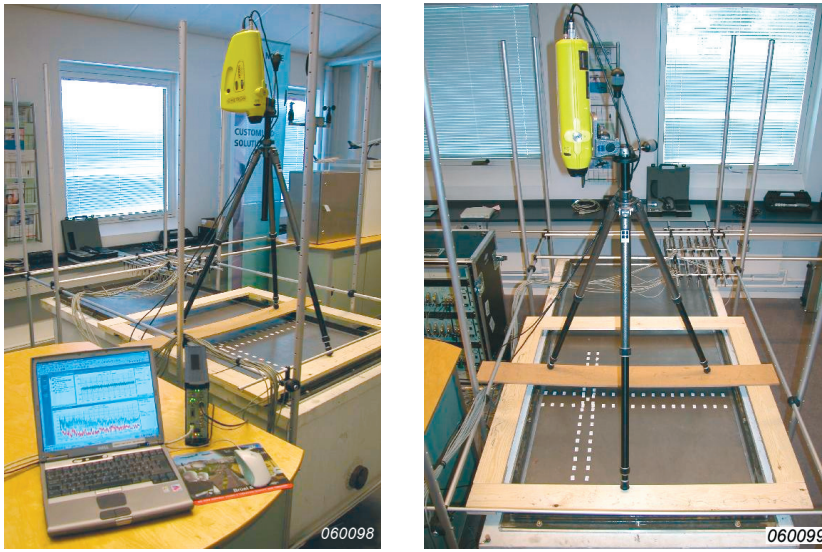

Results and Discussion

Surface normal velocity results obtained with all three methods are compared in two different ways. For a few selected fixed frequencies the spatial distribution of velocity is compared via contour plots. Additionally, for selected fixed positions, corresponding velocity spectra are compared.

Fixed Frequency

The results of Table 1 show that theoretically, the plate under investigation has a resonance frequency at 131 Hz corresponding to the (5,5) mode and another resonance frequency at 151 Hz corresponding to the (5,7) mode. In practice, these resonance frequencies may be shifted somewhat due to, for example, non-ideal boundary conditions compared to the theoretically assumed ones.

Fig. 5 shows an example of surface velocity contour plots obtained using the IBEM (Fig. 5.A), the PNAH (Fig. 5.B) and the LDV (Fig. 5.C) methods at 142 Hz.

The IBEM and PNAH results are nearly identical, showing a clear 5×5 peak velocity pattern. The LDV result has a different colour coding and includes phase

Fig. 5. Surface velocity contour plots of (5,5) mode at 142 Hz obtained with IBEM (A), PNAH (B) and LDV (C)

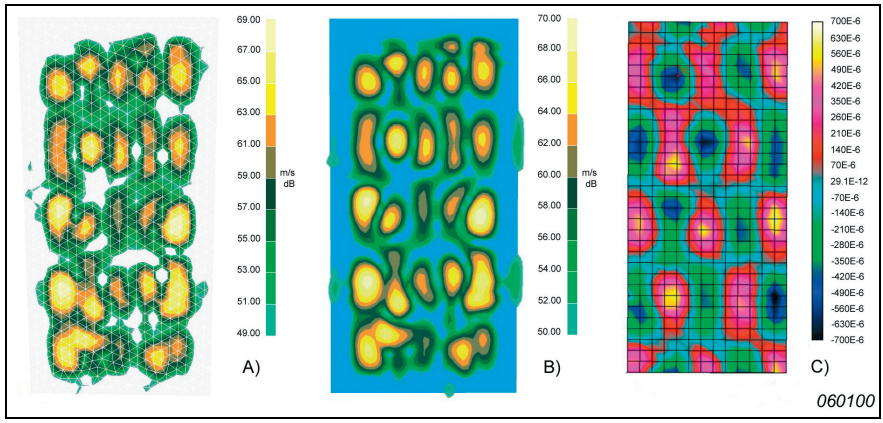

information, but also here a 5×5 peak velocity pattern can be identified. Thus it is reasonable to conclude that all three methods clearly identify the plate (5,5) mode at this frequency.

Fig. 6 shows similar plots at 162 Hz where the (5,7) mode is identified. The qualitative agreement between the results is good in both cases. In particular, the agree-

Fig. 6. Surface velocity contour plots of (5,7) mode at 162 Hz obtained with IBEM (A), PNAH (B) and LDV (C)

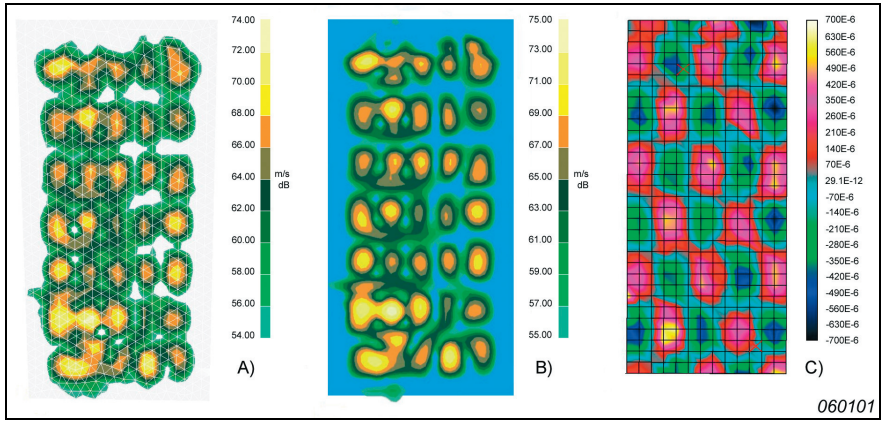

ment between the results obtained with IBEM and PNAH is excellent with detailed information being represented in almost exactly the same way in both cases. The agreement with the velocity distribution obtained with LDV is reasonable, with clear identification of the velocity patterns. Differences between the results obtained with LDV on one hand and IBEM/PNAH on the other may be explained by the fact that the IBEM and PNAH methods provide only an estimate of the surface velocity based on sound radiation. In other words, only the parts of the velocity pattern creating measurable acoustic signals at the receiver microphones may be reconstructed. Moreover, it should be noted that the LDV measurement points were positioned within the boundaries of the plate (see Fig. 8) whereas the IBEM and PNAH methods provide results all the way to (and beyond) the plate border. Also, the LDV results contain phase information which is the reason for the alternating colors in the LDV plots. Finally, sources of error such as position errors and non-freefield conditions may affect the quality of the results.

Comparing the IBEM and PNAH methods to the LDV method, it is already clear that they do not yield identical surface vibration maps since the IBEM and PNAH methods provide only an estimate based on sound radiation. Only the slowly spatially varying (smooth) surface vibration components may be reconstructed by the IBEM and PNAH methods, since the fast varying components generate exponentially decaying acoustic waves that are difficult to pick up and reverse. The obtainable resolution depends on the signal-to-noise ratio of the decaying waves at the microphone positions. This is clearly illustrated by the surface contour plots shown in Fig. 7 corresponding to an example analysis frequency of 974 Hz.

Fig. 7. Surface velocity contour plots at 974 Hz obtained with IBEM(A), PNAH(B) and LDV (C)

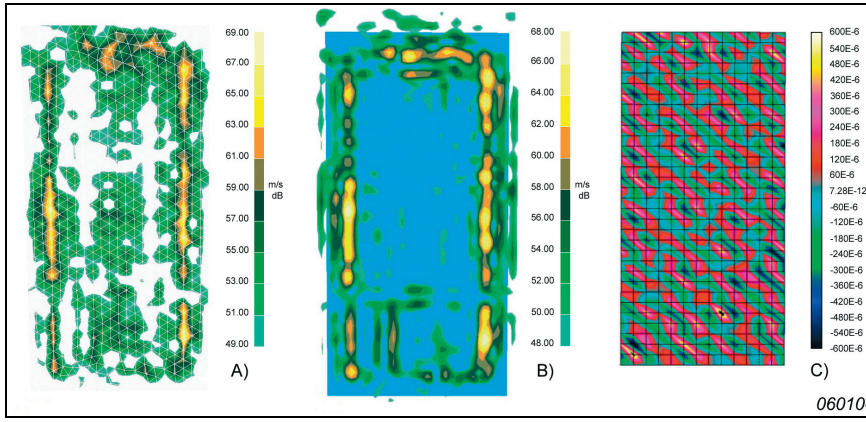

Again, the agreement between IBEM and PNAH is excellent. From these results it appears as if only the borders of the plate are vibrating significantly. However, the LDV method provides a very different result with a very fast spatially varying surface velocity distribution of equal absolute levels throughout the entire plate area. The physical explanation for this discrepancy is that as frequency increases, the structural wavelengths of the plate vibrations become so small compared to the acoustical wavelength that hydrodynamical 'short circuiting' largely prevents the plate from radiating sound efficiently, except at the plate borders where no cancellation takes place. Thus, in the interior of the plate, exponentially decaying waves are emitted that decay below the dynamic range capabilities of the IBEM and PNAH methods, and as a result no vibration is detected in this area. While this phenomenon is also present at the lower example frequencies 142 Hz and 162 Hz, the decay rate of the radiated waves at these frequencies is within the dynamic range of IBEM/PNAH and the surface velocity patterns are thus reconstructed well at these frequencies.

Fixed Position

It is interesting to use LDV as a reference method in order to investigate further the accuracy of the absolute surface normal velocity estimate (as a function of frequency) obtained by the IBEM and PNAH methods. Because of the spatially averaged nature of IBEM and PNAH results, these are not directly comparable to the single-point measurements obtained using LDV. To compensate for this, spatial averaging of the LDV results was applied before comparison.

Two areas on the plate surface were selected for comparison. The first area (A) was positioned in the middle part of the plate while the second area (B) was positioned close to the plate border. The position and size of the areas are shown in Fig. 8. Within each area a number of LDV measurement results were averaged to produce an average velocity level representing the given area. In a similar way average IBEM and PNAH results were obtained by reading off IBEM nodal values and PNAH result values within the area and averaging the data to produce a single value for the given area.

Fig. 9 shows the spatially averaged surface velocity at area A (plate centre) as determined by the IBEM, PNAH and LDV methods.

The agreement between the absolute levels as determined by the three methods is quite good in the frequency range between 30 Hz and 600 Hz. Again, the agreement between IBEM and PNAH is excellent, whereas the agreement between IBEM/PNAH and LDV is characterised by the LDV method giving, in general, slightly higher absolute vibration levels than the other methods. Above 600 Hz the differ-

Fig. 8. Position of comparison areas A and B. Also marked are the LDV measurement points

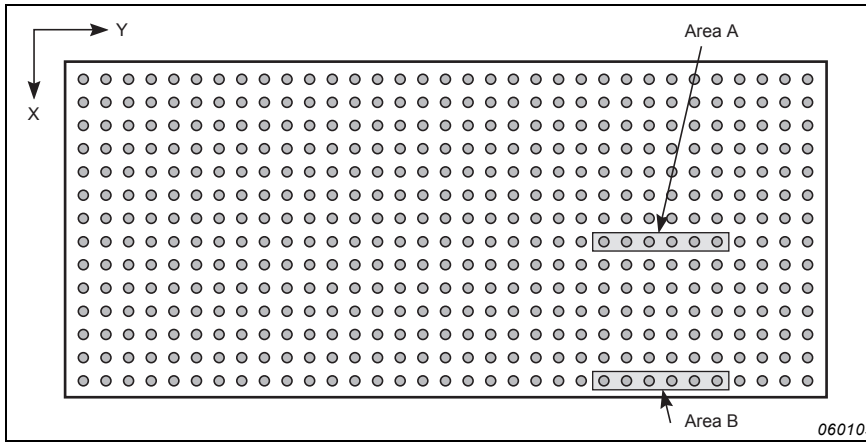

Fig. 9. Comparison of velocity levels determined using IBEM, PNAH and LDV at area A

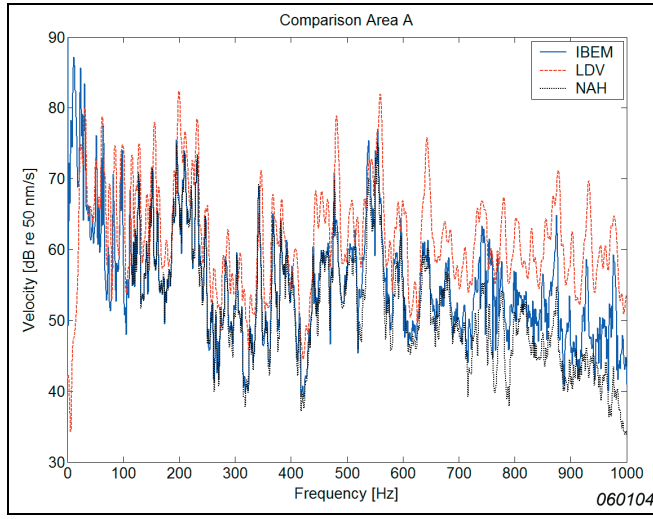

ence in absolute levels between IBEM/PNAH and LDV is more significant. Below 30 Hz, results cannot be compared due to the use of highpass filters in the measurement chains. The upper frequency limit was chosen because of the calculation time of the IBEM method.

Fig. 10 shows the spatially averaged surface velocity at area B (plate border) as determined by the three methods.

Fig. 10. Comparison of velocity levels determined using IBEM, PNAH and LDV at area B

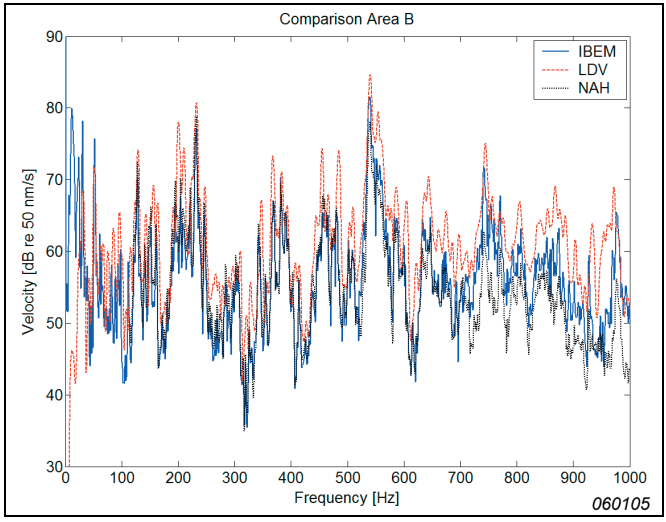

Below 600 Hz the agreement between absolute levels obtained with the three methods follows the same pattern as for area A. However, at frequencies above 600 Hz the differences between levels obtained with IBEM/PNAH and LDV become significantly smaller than those in the case of area A. This is again a consequence of the fact that cancellation of sound radiation takes place in the plate interior but not at the plate border. Thus, at the plate border significant radiation information may be picked up by the microphones, and the agreement between levels at the plate border may therefore be expected to be better than at the plate centre as frequency increases.

Conclusions and Future Work

Two different acoustical holography methods for surface velocity reconstruction have been compared by experiments on a vibrating panel: The Inverse Boundary Element Method (IBEM) and Planar Near-field Acoustical Holography (PNAH). The IBEM method allows for velocity reconstruction on arbitrary 3D surfaces while PNAH is limited to 2D planar surfaces. Although quite different in principle

and implementation the two methods have shown excellent agreement in terms of both spatial velocity distribution and absoulte measured levels. Results obtained with the IBEM and PNAH methods have furthermore been compared to results obtained by the well-established Laser Doppler Vibrometry (LDV) method for non-contact vibration measurement. Good agreement both in spatial distributions and absolute levels has been found in cases where the plate vibration generates sufficient sound field information at the IBEM/PNAH reciever microphones. Conversely, deviations between levels obtained with IBEM/PNAH and with LDV may be explained by the fact that only the part of the plate vibration causing significant radiation may be reconstructed by the holography methods.

The IBEM and PNAH methods provide a limited resolution estimate of the surface velocity from acoustic measurements. This means that for detailed surface velocity analysis the LDV method is superior – especially at high frequencies where the demands on mesh density and microphone spacing in IBEM become prohibitive. However, for overall source location and structure-borne sound analysis, the IBEM method is a viable alternative to LDV. Moreover, the surface BEM solution obtained with IBEM may be used directly in further simulations. Future work will include validation of measurements on industrial applications, for example, on a running car engine.

References

[1] Mørkholt J., Jacobsen N-J., Schuhmacher A., "*Comparison of Scanning Laser Measurement and Inverse Boundary Element Method*", IMAC XXII, 2004.

[2] Jacobsen N-J., Mørkholt J., Schuhmacher A., "*Comparison of Laser Measurement and Inverse Boundary Element Method*", ISMA, 2004.

[3] Von Estorff O., "*Boundary Elements in Acoustics*", WIT Press, 2000.

[4] Williams E.G., "*Regularization Methods for Near-Field Acoustical Holography*", J. Acoust. Soc. Am. 110(4), pp. 1976-1988, 2001.

[5] Schuhmacher A., "*Sound Source Reconstruction Using Inverse Sound Field Calculations*", PhD. Thesis, Report No. 77, Department of Acoustic Technology, Technical University of Denmark, 2000.

[6] Schuhmacher A., Hald J., Rasmussen K.B., Hansen P.C., "*Sound Source Reconstruction Using Inverse Boundary Element Calculations*", J. Acoust. Soc. Am. 113, pp. 114-127, 2003.

[7] Hald J., "*STSF – A Unique Technique for Scan-based Near-field Acoustical Holography Without Restriction on Coherence*", Brüel & Kjær Technical Review No. 1, Brüel & Kjær, 1988.

[8] Hald J., "*Patch Near-field Acoustical Holography using a New Statistically Optimal Method*", Proc. Inter-Noise 2003, pp. 2203-2210.

[9] Fahy F., "*Sound and Structural Vibration*", Academic Press, 1985.

Previously issued numbers of Brüel & Kjær Technical Review

(Continued from cover page 2)

1 – 1990 The Brüel & Kjær Photoacoustic Transducer System and its Physical Properties
2 – 1989 STSF — Practical Instrumentation and Application
Digital Filter Analysis: Real-time and Non Real-time Performance
1 – 1989 STSF — A Unique Technique for Scan Based Near-Field Acoustic Holography Without Restrictions on Coherence
2 – 1988 Quantifying Draught Risk
1 – 1988 Using Experimental Modal Analysis to Simulate Structural Dynamic Modifications
Use of Operational Deflection Shapes for Noise Control of Discrete Tones
4 – 1987 Windows to FFT Analysis (Part II)
Acoustic Calibrator for Intensity Measurement Systems
3 – 1987 Windows to FFT Analysis (Part I)
2 – 1987 Recent Developments in Accelerometer Design
Trends in Accelerometer Calibration
1 – 1987 Vibration Monitoring of Machines
4 – 1986 Field Measurements of Sound Insulation with a Battery-Operated Intensity Analyzer
Pressure Microphones for Intensity Measurements with Significantly Improved Phase Properties
Measurement of Acoustical Distance between Intensity Probe Microphones
Wind and Turbulence Noise of Turbulence Screen, Nose Cone and Sound Intensity Probe with Wind Screen

Special technical literature

Brüel & Kjær publishes a variety of technical literature which can be obtained from your local Brüel & Kjær representative.

The following literature is presently available:

- Catalogues (several languages)
- Product Data Sheets (English, German, French,)

Furthermore, back copies of the Technical Review can be supplied as listed above. Older issues may be obtained provided they are still in stock.

HEADQUARTERS: DK-2850 Nærum · Denmark
Telephone: +45 45 80 05 00 · Fax: +45 45 80 14 05
www.bksv.com · info@bksv.com

Brüel & Kjær

BV 0058 – 11 ISSN 0007–2621